VORTEX-INDUCED VIBRATION OF THE UPSTREAM CYLINDER OF A TWO-CYLINDER SYSTEM IN CRUCIFORM ARRANGEMENT

MASATAKA SHIRAKASHI[1], TSUTOMU TAKAHASHI[1], ISAO KUMAGAI[1] AND TSUYOSHI MATSUMOTO[2]

[1]Nagaoka University of Technology, Department of Mechanical Engineering, [2]Mitsubishi Heavy Industry Co. Ltd

1603-1 Kamitomiokamachi, Nagaoka, 940-2188 Japan

kumapu@stn.nagaokaut.ac.jp

Abstract. Comprehensive wind tunnel experiments are carried out on the longitudinal vortex excitation of the upstream cylinder in a cruciform two-cylinder system. The vortex structure around the crossing is dominated by the ratio of gap s to the downstream cylinder diameter d_2, i.e., the trailing vortices shed when $s/d_2 < 0.25$ and the necklace vortices shed when $0.25 < s/d_2 < 0.7$. Based on measurements under variable damping factor, criteria for occurrence of the longitudinal vortex excitations are presented and substantial alternating lift coefficients are proposed for them to estimate the excitation force. These results are of practical importance to predict and to avoid these newly found vortex excitations.

Keywords: Vortex excitation, cruciform arrangement cylinders, longitudinal vortex, scruton number, alternating lift coefficient.

1. Introduction

It is well known that nearly two dimensional vortices shed alternately from both sides of a cylindrical body set in a uniform flow, which form two arrays of vortices in a staggered arrangement in the wake, i.e., Kármán's vortex street [1]-[4]. Since the periodic shedding of Kármán vortex can induce large cross-flow oscillation and/or sound emission which are usually undesirable from the practical point of view, numerous works have been carried out to control the Kármán vortex shedding and in turn the sound and oscillation. Inspired by Tomita et al.'s work [5] on sound depression effect of another cylinder set downstream in a cruciform arrangement as shown in Figure 1, the present authors investigated the oscillation suppressing effect of the downstream cylinder in the same arrangement [6]-[9]. Although the Kármán vortex excitation was eliminated when the cylinder diameters were equal and the gap between the cylinders was less than half the cylinder diameter, a new oscillation was found to occur over a certain velocity range around three times higher than the Kármán vortex excitation [6]. Recent investigations showed that the newly found oscillation is caused by one of two types of vortices which shed periodically around the crossing of the two cylinders, as seen in Figure 2 [7],[10],[11]. They are classified into longitudinal vortices since they have axes parallel to the free flow. Each of them is referred to as the *Trailing vortex* (Figure 2(a)) and the *Necklace vortex* (Figure 2(b)) according to their geometry.

Since very few works have been carried out on these longitudinal vortices and little is known about their nature concerning the vortex excitation yet, it is a problem of practical importance to clarify the characteristics of these longitudinal vortices and to know the conditions under which the longitudinal vortex shedding occurs, and to establish a way to predict the oscillation amplitude for given conditions.

Therefore, the objectives of this work are to obtain understanding of the global nature of the longitudinal vortices, to find a criterion for the occurrence of the vortex excitation and to estimate the exciting force due to the longitudinal vortices, based on comprehensive wind tunnel experiments.
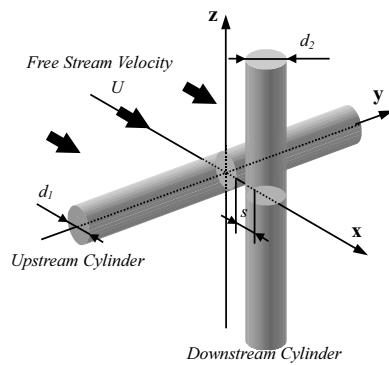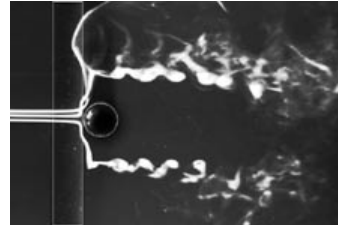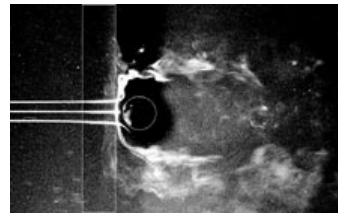

(a) Trailing vortex (U=12.8cm/s, s/d=0.08, Re=860)

(b) Necklace vortex (U=12.5cm/s, s/d=0.28, Re=900)

Figure 1. Arrangement of two cylinders and coordinate system.

Figure 2. Photographs of longitudinal vortices shedding from two cylinders in cruciform arrangement. (in water tunnel, $d = d_1 = d_2 = 10$mm)

2. Nomenclature

A	oscillation amplitude of the upstream cylinder $= \sqrt{2} \cdot Z_{rms}$
$(C_L)_{rms}$	fluctuating lift coefficient, equation (4.1)
$(C_L)'_{rms}$	substantial fluctuating lift coefficient, equation (4.2)
$(C_{LR})_{rms}$	alternating lift coefficient, equation (4.4)
$(C_{LR})'_{rms}$	substantial alternating lift coefficient, Equation (4.5a, 4.5b)
d	cylinder diameter in case of identical cylinder system, i.e. $d = d_1 = d_2 = 26mm$
f	frequency
f_c	oscillation frequency of the upstream cylinder
f_n	natural frequency of the elastically supported upstream cylinder

f_v	vortex shedding frequency
f_{v0}	vortex shedding frequency from a fixed system
l	effective length of cylinder
Re	Reynold's number defined by $Re = U \cdot d_1/\nu$, where ν is the kinematic viscosity of air
s	gap between cylinders
Sc	Scruton number defined by equation (4.3)
St	Strouhal number for the vortex shedding frequency defined by $St = f_v \cdot d_1/U$
St_0	Strouhal number for the fixed system defined by $St_0 = f_{v0} \cdot d_1/U$
St_2	Strouhal number referred to d_2
S_L, Su	spectrum of lift force and velocity, respectively
Su_{AB}	cross spectrum of velocities detected at two positions A and B
$(Su_{AB})_{peak}$	maximum peak value of Su_{AB}
U	free flow velocity
U_0	the free flow velocity at which $f_{v0} = f_n$
Z_{rms}	root-mean-square value of z-displacement of the upstream cylinder
δ	logarithmic damping factor

3. Experimental apparatus and procedures

The arrangement of the two cylinders, the coordinate system and symbols used in this paper are shown in Figure 1. The wind tunnel is a blow down type. The maximum attainable velocity is 40 m/s and the turbulence intensity is less than 0.4% at 10 m/s. The measuring section is 320 mm*320 mm in cross-section and 1000 mm in length. The upstream cylinder is set horizontally and perpendicularly to the free flow at the center of the measuring section. It passes through the slots on the sidewalls of the measuring section. End plates are fixed on the cylinder near both ends to avoid flow through the slots. The downstream cylinder is fixed vertically on a traverse device so as to make the gap s adjustable within an error of 0.01 mm. On the details of the apparatus, see [6].

The diameter of the downstream cylinder d_2 is varied from 18 mm to 32 mm, while the upstream cylinder diameter d_1 is fixed at 26 mm. The effective length l of the cylinder, i.e. the distance between the two end plates, is also fixed at 318 mm. Experiments are conducted first for a system with two identical cylinders, i.e. $d_1 = d_2$, and then influence of the diameter ratio d_2/d_1 is investigated. Hence, the diameters of both cylinders are simply denoted as d when the two cylinders are identical. In the following sections the diameters of both cylinders are equal at 26 mm whenever d is used as the cylinder diameter.

The upstream cylinder is fixed rigidly, or supported elastically by plate springs outside the measuring section. In the latter case, the motion of the elastically supported cylinder is almost purely translational in vertical ($z-$) direction. An eddy-current damper is applied to the elastically supported system to adjust the logarithmic damping factor δ from 0.008 to 0.2. The natural frequency f_n of the elastic system and the damping factor are determined from a free damping oscillation experiment in other-

wise quiescent air. A mechanical oscillator is used to oscillate the upstream cylinder sinusoidally in vertical direction with an arbitrary amplitude and frequency.

The free flow velocity U is measured by a ring type Kármán vortex velocimeter developed in the present authors' laboratory [12].

Hot wire anemometry is applied to detect u, the x-component of velocity fluctuation. Two hot wire probes, probe A and B, are set at opposite sides of the upstream cylinder near the crossing to detect the velocity fluctuation caused by the periodic vortex shedding. The positions of probes are determined by moving them to find places where the fluctuation component due to the longitudinal vortex shedding is most clearly discerned. The probe positions thus determined depend on the conditions such as the gap-to-diameter ratio and the downstream cylinder diameter, as indicated in the captions of figures. The vortex shedding frequency f_v is determined from the cross spectrum Su_{AB} of two velocity signals u_A and u_B. The relative peak height of Su_{AB} at f_v is considered to be a measure of the strength or regularity of the vortex, although that value of the height itself has no significance. By using the cross spectrum and its peak value, phenomena concerning the longitudinal vortices are discerned more definitely than only to depend on one velocity signal as applied so far.

The displacements at both ends of the upstream cylinder are measured by a non-contacting laser beam displacement detector within an error of 0.1 mm over a range of 0-13 mm.

The lift force acting on the fixed upstream cylinder is measured using a strain-gauge type load-cell.

4. Results and discussion

4.1. Characteristics of longitudinal vortices shedding from fixed system

4.1.1. *Influences of gap-to-diameter ratio and Reynolds number for identical-cylinder system.* In this section, results obtained for a system with an equal diameter two cylinders, i.e. $d_1 = d_2 = 26$ mm $(=d)$, are presented. Figure 3 shows the cross spectra of velocities detected at two positions around the crossing of the cylinders for various values of the gap-to-diameter ratio s/d under a fixed velocity. The two probe positions A and B are symmetrical with each other about the $x-y$ plane. Note that these probe positions are selected because they are most suitable to detect the periodic shedding of the respective longitudinal vortices. It is clearly seen that the shape of cross spectrum Su_{AB} and the peak frequency are definitely different between two regions of s/d, noted as the region T $(s/d = 0 - 0.25)$ and the region N $(s/d = 0.25 - 0.64)$. Strouhal numbers of these peak frequencies correlate well with those confirmed for the longitudinal vortex shedding frequencies based on various measurements, including counting the vortex shedding in the visualized flow, as shown in Figure 2.

The vortex shedding frequency f_{v0} is determined as the highest-peak frequency of Su_{AB}. In Figure 4 the Strouhal number St_0 for the vortex shedding frequency f_{v0} is plotted against s/d for various Reynolds numbers. The abrupt change at $s/d = 0.25$

observed in the earlier works is confirmed more clearly in this figure. The $St_0 - s/d$ curve of the trailing vortex ($s/d < 0.25$) has an irregular shape and depends largely on the Reynolds number in a somewhat incoherent way, while that of the necklace vortex ($s/d > 0.25$) collapses on a single curve. The maximum value of s/d for the necklace vortex shedding is shown to be 0.7, which is considerably larger than in the earlier works.

The peak value of Su_{AB} at f_{v0} is plotted against s/d in Figure 5 for various values of free flow velocity U. It is confirmed again in this figure that $s/d = 0.25$ is the boundary value separating the trailing vortex region and the necklace vortex region. In the earlier works by the authors, $s/d = 0.08$ and $s/d = 0.28$ were used as the representative values for the trailing vortex and the necklace vortex since the shedding of the two vortices were observed to shed most regularly at these values of s/d [8]. Since $(Su_{AB})_{peak}$ in Figure 5 has the local maximum value for these values of s/d in the respective regions, these s/d values are selected also in this work as the representatives for the two longitudinal vortices.
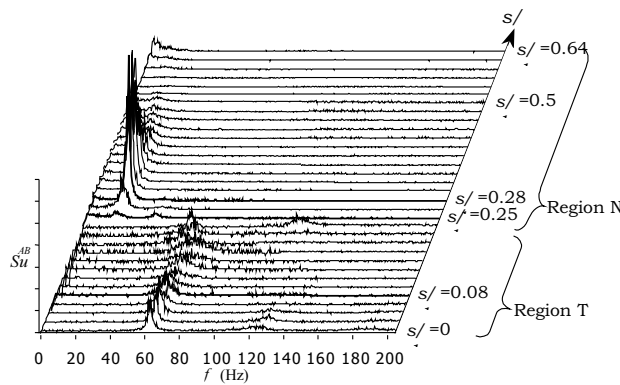

Figure 3. Cross-spectra of velocities at two locations around the crossing for various values of s/d. ($U = 8.0 \ m/s, Re = 14,000$) Probe position: Region T ($x/d = 0.5, \ y/d = -1.25, \ z/d = 0.5 \ or -0.5$) Region N ($x/d = 0.5, \ y/d = -0.75, \ z/d = 0.5 or -0.5$)

Strouhal numbers for the two longitudinal vortices at the above representative s/d values are plotted against Reynolds number in Figure 6, where the ranges of the results reported so far are compared. The Strouhal number for the necklace vortex increases continuously with Re when $500 < Re < 5,000$ and attains at a value around 0.04, then decreases very gradually up to $Re = 40,000$. Meanwhile, the Strouhal number for the trailing vortex increases with Re over the whole Re range of measurement, and has a discontinuous jump at Re around 5,000.

The results in this section as shown in Figures 3, 4 and 6 show the different natures of the two longitudinal vortices. The structure of flow near the crossing is definitely decided by the gap-to-diameter ratio, i.e., the trailing vortices shed when $s/d < 0.25$

and the necklace vortices when $0.25 < s/d < 0.7$ over a wide range of Reynolds number Re. The necklace vortex has a regular and definite nature in that the Strouhal number St_0 is nearly constant over the Reynolds number range 5,000 to 40,000 and that $St_0 - s/d$ data for various Re collapse on a single curve which decreases gradually with s/d. In contrast, St_0 for the trailing vortex increases from 0.02 to 0.09 in the same Re range, and the $St_0 - Re$ curve has a discontinuous jump at around $Re = 5,000$. The change of St_0 with s/d is quite large and irregular, and the influence of Re on the $St_0 - s/d$ relationship is not coherent. Besides, the peak value of the cross spectrum for the trailing vortex is usually lower than that for the necklace vortex as seen in Figure 3, showing that the periodicity of the trailing vortex shedding is less than that of the necklace vortex.
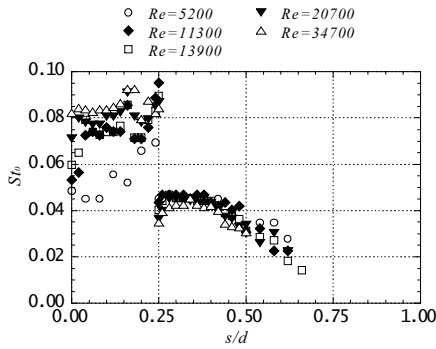

Figure 4.   Relationship between Strouhal number and gap-to-diameter ratio for various Reynolds numbers for longitudinal vortices.   (fixed system, $d = d_1 = d_2 = 26\ mm$)
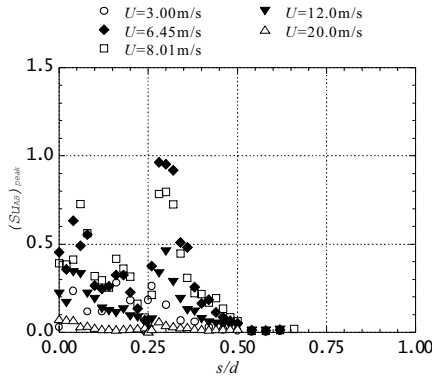
Figure 5. Peak values of cross-spectrum vs. gap-to-diameter ratio. (fixed system, $d = d_1 = d_2 = 26$ mm)

4.1.2. *Influence of diameter ratio.* Figure 7 shows the vortex shedding frequency f_{v0} plotted against the downstream cylinder diameter d_2 in a system where the two cylinders are not identical. While f_{v0} of the necklace vortex at a fixed free flow velocity decreases with d_2 for all the values of the gap, there was found no systematic tendency in the influence of d_2 on f_{v0} on the trailing vortex. Taking this behavior of the necklace vortex into consideration, the downstream cylinder diameter is taken as the reference length to define the Strouhal number, i.e. $St_2 = f_{v0} \cdot d_2/U$. In Figure 8, St_2 is plotted against the gap s divided by d_2 for several diameter ratios. In this figure it is clearly seen that St_2 changes abruptly at $s/d_2 = 0.25$, and the $St_2 - s/d_2$ relation is clearly different between the two regions bounded by this value of s/d_2, like in Figure 4 for the identical cylinder system. This result suggests that the downstream cylinder diameter has the decisive effect on the vortex structure around the crossing. However, St_2 plotted against s/d_2 scatters largely for the trailing vortex ($s/d_2 < 0.25$) and does not collapse well on a single curve for the necklace vortex ($0.25 < s/d_2 < 0.5$).
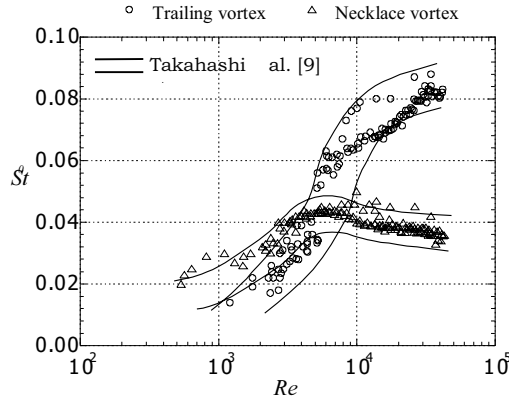
Figure 6. Relationship between Strouhal number and Reynolds number for the longitudinal vortices. (fixed system, $d = d_1 = d_2 = 26$ mm) Trailing vortex : $s/d = 0.08$, Necklace vortex : $s/d = 0.28$
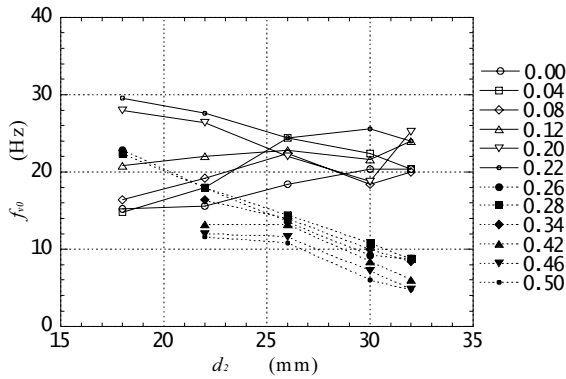

Figure 7. Relationship between the vortex shedding frequency and the downstream cylinder diameter. (fixed system, $U = 8.0 \ m/s$, $Re = 14,000$)

To see the span-wise size of the longitudinal vortices, a hot wire probe is moved parallel to the upstream cylinder axis. Figure 9 shows the spectrum Su of the velocity detected by the probe for the identical cylinder system at various values of y/d. The gap is set at the representative values for (a) the trailing vortex and (b) the necklace vortex. In Figure (a), near the downstream cylinder, say $y/d < 2.4$, Su has the highest peak corresponding to the trailing vortex, and the maximum value of y/d at which the trailing vortex peak is observed is $y/d = 3.2$. At larger values of y/d, the Kármán vortex peak becomes dominant in a spectrum. From this figure, the span-wise extent of the trailing vortex is estimated around $y/d = 3.2$, as indicated in the figure as R_T. The span-wise extent R_N of the necklace vortex is also determined in

the same manner from Figure 9(b). R_T and R_N thus obtained are regarded as the measures of the span-wise size of the trailing and the necklace vortices, respectively. It is confirmed that R_T is considerably larger than R_N as observed in the photographs
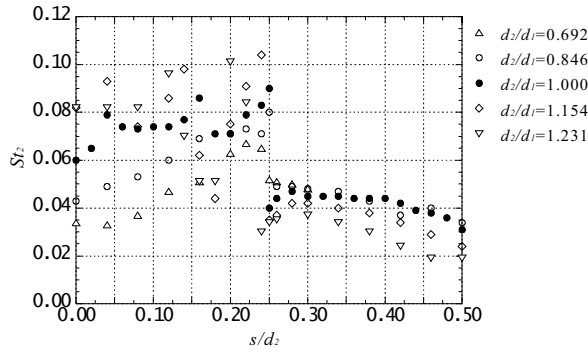

Figure 8. Relationship between Strouhal number and gap-to-diameter ratio referred to the downstream cylinder diameter. (fixed system, $U = 8.0$ m/s, $Re = 14,000$)
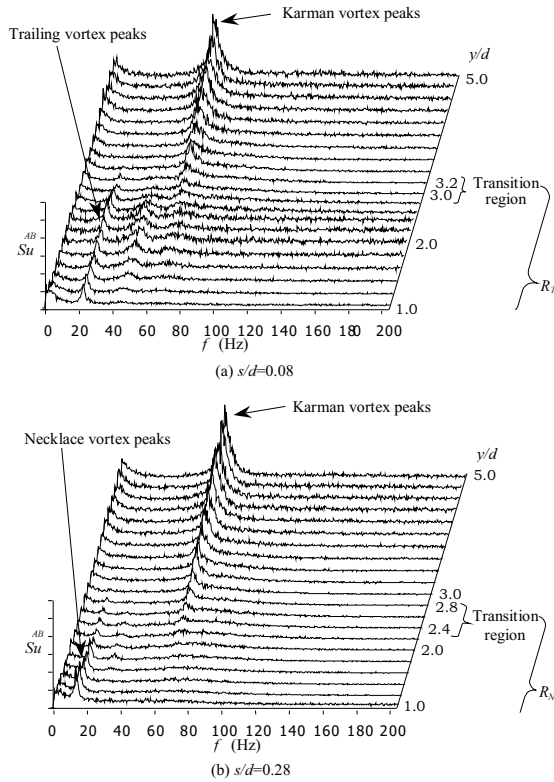

Figure 9. Variation of linear spectrum of velocity along the span wise direction of upstream cylinder. (fixed system, $d = d_1 = d_2 = 26$ mm, $U = 8.0$ m/s, $Re = 14,000$)

of the visualized vortices in Figure 2. Measurements on systems with various d_2/d_1 show that the span wise size of the two longitudinal vortices are roughly proportional to the downstream cylinder diameter.

4.1.3. *Fluctuating lift force acting on the upstream cylinder.* Oscillograms of the fluctuating lift force acting on the upstream cylinder in the identical cylinder system and its spectrum S_L are shown for $s/d = 0.08$, 0.25 and 0.28 in Figure 10. Velocities at the two reference positions, u_A and u_B, were measured simultaneously. At $s/d = 0.08$ and 0.28, a dominant frequency component is observed and the frequency of this dominant component is shown to coincide with the vortex shedding frequency f_{v0} determined from the velocity cross spectrum Su_{AB} for the respective values of s/d. At $s/d = 0.25$, two peaks appear in S_L corresponding to the trailing and the necklace vortices. The oscillogram shows that the two vortices shed not simultaneously but alternately at $s/d = 0.25$.

The lower peak in S_L at $f = 75$ Hz which appears for the three values of s/d is due to the Kármán vortex shedding.
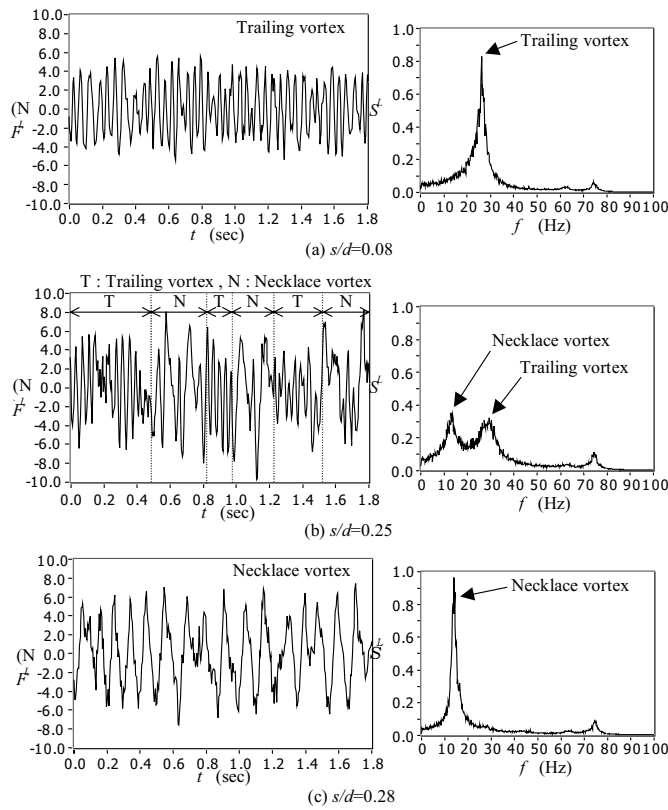

Figure 10. Oscillograms and spectra of fluctuating lift force on the upstream cylinder (fixed system, $d = d_1 = d_2 = 26$ mm, $U = 8.0$ m/s, $Re = 14,000$)

The root-mean-square value of the fluctuating lift coefficient $(C_L)_{rms}$ is calculated from the measured root-mean-square value of lift, $(F_L)_{rms}$, using equation (4.1) and plotted against Re in Figure 11.

$$(C_L)_{rms} = \left[(F_L)_{rms} / \frac{1}{2}\rho U^2 ld \right] . \qquad (4.1)$$

$(C_L)_{rms}$ of the Necklace vortex is nearly constant over the Reynolds number range from 5,000 to 30,000, while that of the trailing vortex decreases by the factor of two over the same Re range.
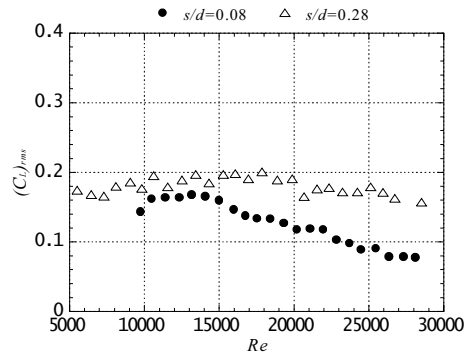

Figure 11. Fluctuating lift coefficient due to the longitudinal vortices (fixed system, $d = d_1 = d_2 = 26\ mm$)
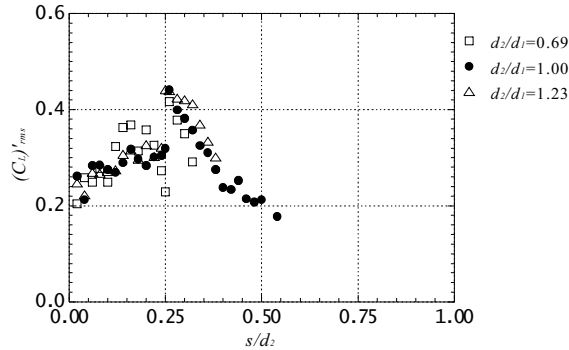
Figure 12. Substantial fluctuating lift coefficient vs. gap-to-diameter ratio (fixed system, $U = 8.0$ m/s, $Re = 14,000$, $d_1 = 26\ mm$)

The alternating lift force is the resultant of the fluctuating pressure acting on the upstream cylinder surface caused by the periodical shedding of longitudinal vortices. The measurement of span-wise size of the longitudinal vortices as presented in Figure 9 shows that the fluctuating pressure due to the longitudinal vortices is exerted on

a limited part of the effective length of the upstream cylinder. $(C_L)_{rms}$ defined by equation (4.1) is based on the assumption that the lift force distributes uniformly over the whole span of the upstream cylinder. A practical improvement to define the lift coefficient is to use the real span wise length of the longitudinal vortices as given by R_T and R_N in Figure 9. Therefore, the substantial fluctuating lift coefficient is defined by the following equation

$$(C_L)'_{rms} = \left[(F_L)_{rms} / \frac{1}{2} \rho U^2 d \times 2R_T \ (or \ R_N) \right] . \quad (4.2)$$

$(C_L)'_{rms}$ thus obtained are plotted against s/d_2 in Figure 12 for three values of d_2/d_1. Figure 12 shows that the alternating lift force due to the longitudinal vortices is nearly proportional to their span wise extent along the upstream cylinder, and hence proportional to d_2 in turn.

Results in Figures 9 and 12 give a guide to estimate the fluctuating lift force exerted on the upstream cylinder when dimensions of a cruciform cylinder system, d_1, d_2 and s, and flow velocity are given.

4.2. Oscillation behavior of the upstream cylinder

The cross flow oscillation behavior of the upstream cylinder is observed when the free flow velocity is stepwisely increased and then decreased. In Figure 13, the rms value of the z-displacement of the upstream cylinder and the vortex shedding frequency f_v are plotted against the free flow velocity U. The vortex shedding frequency from the fixed equivalent, f_{v0}, and the natural frequency of the elastically supported upstream cylinder, f_n, are presented for comparison. Similarly to the well known Kármán vortex excitation, very large oscillations are caused by the two longitudinal vortices over a certain velocity range, always accompanied by the synchronization phenomenon of the vortex shedding with the cylinder oscillation. "Over range" means that the oscillation amplitude is beyond the range of measurement. The spectrum S_Z of the displacement shows that the frequency of these large excitations and hence the vortex shedding frequency f_v, coincide with the natural frequency f_n of the cylinder.

Outside the excitation region, the vortex shedding frequency f_v is nearly equal to f_{v0}, and S_Z has a maximum peak at $f = f_n$ irrespective of U, showing that the cylinder always oscillates at its natural frequency f_n. When U is a little higher than the vortex excitation range, an additional peak appears in S_Z at f_v. In this case, a beat motion is observed in the oscillogram of the cylinder displacement.

The vortex excitation regions expand around the velocity U_0, the velocity at which the vortex shedding frequency f_{v0} from the fixed equivalent is equal to the natural frequency f_n of the elastically supported system. A hysteresis behavior is also observed clearly in the necklace vortex excitation and less clearly but definitely for the trailing vortex excitation as seen in Figures 13(a) and (b), respectively. The different features between the two longitudinal vortex excitations are clearly observed as follows.

In Figure 13(a), the velocity range of the trailing vortex excitation expands to a value as low as one half of U_0, and it is narrower for U higher than U_0. Accordingly, the jump of f_v caused by the synchronization at the lower edge of the excitation range is very large. This may be associated with the jump of f_{v0} in the $f_{v0} - U$ curve which
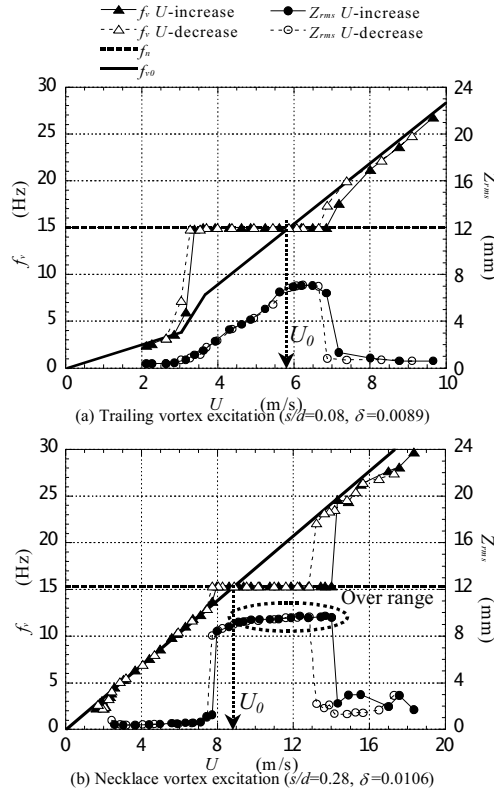
Figure 13. Relationship between oscillation amplitude and flow velocity. ($f_n = 15\ Hz$, $d = d_1 = d_2 = 26\ mm$)

results in the discontinuity in the $St_0 - Re$ relationship in Figure 6. In spite of this large jump of f_v at the lower edge of vortex excitation range, the change of oscillation amplitude there is continuous and the amplitude increases rather gradually with U in the excitation range up to $U = U_0$. In contrast, the necklace vortex excitation region starts at a velocity slightly lower than U_0 and the excitation region expands to a velocity much higher than U_0, as seen in Figure 13(b). In spite of the slight jump in f_v at the lower edge of the excitation region, the oscillation amplitude abruptly increases with a large step there.

In Figure 14, the relationship between the oscillation amplitude and the gap-to-diameter ratio under a fixed flow velocity is presented for various diameter ratios. The two values of flow velocity U in the figure are selected as the representatives of the trailing vortex excitation ($U = 7.0$ m/s) and the necklace vortex excitation ($U = 12.0$ m/s) in Figure 13. When $U = 7.0$ m/s, the oscillation is large in the region $s/d_2 < 0.25$ and almost disappears for s/d_2 larger than the boundary value of s/d_2, except the case of $d_2/d_1 = 0.692$. Since the cylinder oscillates at its natural frequency

f_n and f_{v0} of the trailing vortex at this velocity is close to f_n, the vortex shedding is "locked in" the cylinder oscillation and the oscillation amplitude becomes large due to the resonance, i.e. the trailing vortex excitation. In contrast, large excitations occur in the region $0.25 < s/d_2 < 0.75$ when $U = 12.0$ m/s. Since the natural shedding frequency f_{v0} of the necklace vortex at this velocity is close to the natural frequency f_n of the cylinder, this oscillation is attributed to the necklace vortex excitation.

The abrupt change of oscillation amplitude at around $s/d_2 = 0.25$ means that a very slight change of the gap can induce a large oscillation. Generally speaking, the maximum cylinder oscillation amplitude is larger when the downstream cylinder diameter d_2 is larger.
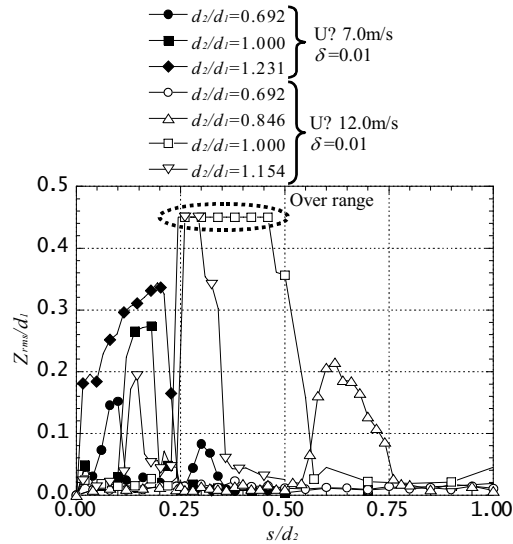

Figure 14. Oscillation amplitude vs. non-dimensional gap for various diameter ratio ($\delta = 0.01$, $d_1 = 26$ mm, $f_n = 14.8$ Hz)

In some cases large oscillations appear in the two regions of s/d_2, as the case of $d_2/d_1 = 0.692$ at $U = 7.0$ m/s and $d_2/d_1 = 1.154$ at $U = 12.0$ m/s. This behavior is explained by the result shown in Figure 8. For example, St_2 for $d_2/d_1 = 0.692$ in Figure 8 has an equal value in the both regions of the trailing vortex ($s/d_2 < 0.25$) and the necklace vortex ($s/d_2 > 0.25$). Hence, the natural vortex shedding frequency f_{v0} is equal to f_n in the two regions of s/d_2. Therefore, the vortex shedding synchronizes with the cylinder oscillation and the vortex excitation occurs in the two regions of s/d_2, i.e. two maximum peaks appear in the $Z_{rms}/d_1 - s/d_2$ curve for $d_2/d_1 = 0.692$ as seen in Figure 14.

Results shown in Figures 13 and 14 are well coherent with the results on the fixed systems, confirming that a large oscillation is induced by either of the two longitudinal vortices in the respective regions of s/d_2.
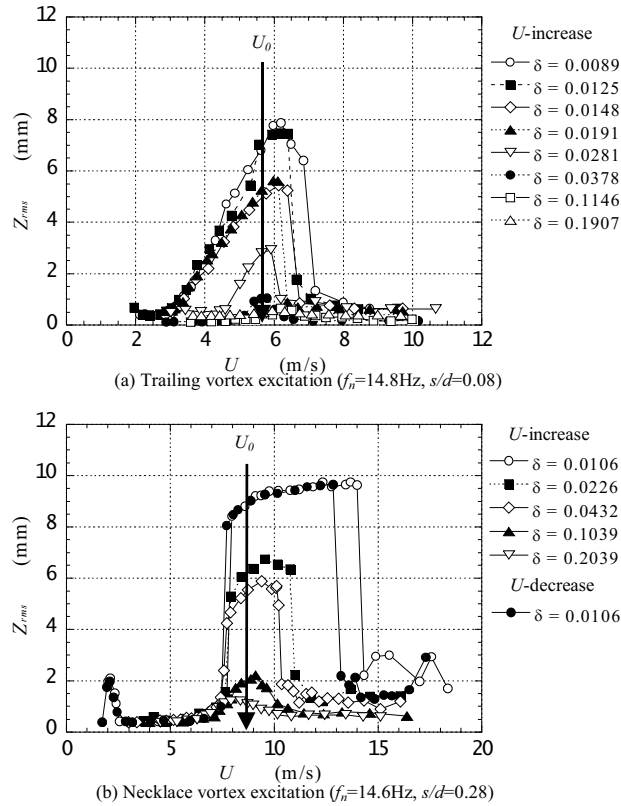
(a) Trailing vortex excitation (f_n=14.8Hz, s/d=0.08)

(b) Necklace vortex excitation (f_n=14.6Hz, s/d=0.28)

Figure 15. Effect of damping factor on oscillation-velocity curve. ($d = d_1 = d_2 = 26\ mm$)

Figure 15 shows the effect of the damping factor on the longitudinal vortex excitations. When δ is increased, the oscillation amplitude decreases for both of the two longitudinal vortex excitations. The width of the velocity range of vortex excitation shrinks towards U_0, the velocity at which $f_{v0} = f_n$. For all the measured values of the damping factor, the maximum amplitude of trailing vortex excitation occurs at U_0, while that for the necklace vortex appears at U considerably higher than U_0.

The hysteresis behavior is not discernible for damping factors larger than those in Figure 13.

4.3. Lock-in phenomenon of the longitudinal vortex

Although the synchronization of the vortex shedding with the upstream cylinder oscillation (lock-in) occurs with the vortex excitation, it is not essential for the lock-in whether the oscillation is induced by the fluid force or not. The lock-in is a phenomenon in the flow caused by the cylinder oscillation irrespective of the mechanism of the cylinder motion. When the vortex shedding is said to "lock-in" the cylinder oscillation,

it is controlled by the cylinder oscillation so that the vortex shedding frequency f_v coincides with the cylinder oscillation frequency f_c and the velocity fluctuation caused by the vortex shedding is in phase with the cylinder displacement, consequently its periodicity becomes more regular. When the cylinder oscillation amplitude is smaller than a certain value, it cannot control the vortex shedding. The threshold value of amplitude for the lock-in is investigated using a mechanical oscillator [13]. The results are presented by the broken lines in Figure 16 where the abscissa expresses the ratio of the cylinder oscillation frequency to the natural vortex shedding frequency and the coordinate the relative amplitude of the cylinder oscillation. The lock-in threshold has a finite value even when $f_c/f_{v0} = 1$. It means that the vortex shedding is not controlled by a cylinder oscillation with an amplitude smaller than this threshold value even when the cylinder oscillation frequency is equal to the natural vortex shedding frequency.

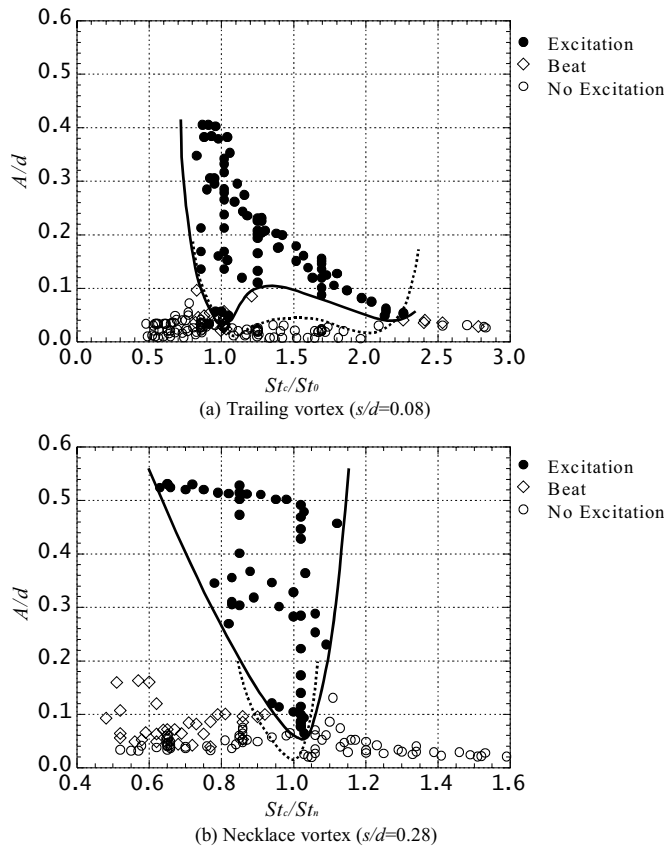(a) Trailing vortex (s/d=0.08)

(b) Necklace vortex (s/d=0.28)

Figure 16. Synchronization region and excitation region for the longitudinal vortices. ($d = d_1 = d_2 = 26\ mm$) Solid curve: Contour of excitation region. Broken curve: Contour of lock-in region measured by mechanical oscillator

The regions of the vortex excitation for the two longitudinal vortices are also presented in Figure 16. The solid lines express the contour of the region where the vortex excitations are observed. The vortex excitation regions observed for the elastically supported system seem to be included in the above lock-in regions for the respective vortices. The symbol "Beat" means that the cylinder oscillation contains both f_n and f_v components but the amplitude is very small, as mentioned in Section 4.2.

The lock-in region for the necklace vortex (Figure 16(b)) is understandable from the phenomenological point of view in that the lock-in threshold is minimum at $f_c = f_{v0}$ and it increases rapidly when f_c differs from f_{v0} in both sides of f_{v0}. However, for the trailing vortex (Figure 16(a)) the lock-in region expands to very large values of $f_c/f_{v0} > 1$ and the threshold amplitude does not increase monotonouosly but has a second minimum value at around $f_c/f_{v0} = 2$. This peculiar behavior of the trailing vortex is not understood at present, but may be associated with the lock-in region widely expanding to a velocity lower than U_0 and the discontinuity in $f_{v0} - U$ curve in Figure 13.

Since the lock-in phenomenon is the feedback of flow to the cylinder oscillation which plays an essential role in the vortex excitation, it is acutely desired to clarify the conditions for the lock-in by appropriate non-dimensional parameters as shown in Figure 16. It is also desired to clarify the influences of other parameters, i.e. Reynolds number, gap-to-diameter ratio and diameter ratio of the two cylinders, on the contour lines in Figure 16.

4.4. Criterion for the longitudinal vortex excitation and estimation of the alternating lift force

From an engineering point of view, the most practical way to avoid the vortex excitation is to make the natural frequency of the system far enough from the vortex shedding frequency f_{v0} and/or to adopt a damping factor large enough to suppress the oscillation. Hence, in order to predict occurrence of vortex excitations of a system, it is a convenient way to present the vortex excitation range of f_{v0} at an arbitrary damping factor. To generalize the expression, these parameters are non-dimensionalized into the relative deviation of f_{v0} from f_n, i.e. $(f_{v0} - f_n)/f_n$, and the Scruton number as defined by the following equation [14].

$$Sc = 2m\delta/\rho d^2 l \,. \tag{4.3}$$

Occurrence of the longitudinal vortex excitations is expressed on the $Sc - (f_{v0} - f_n)/f_n$ plane in Figure 17 , where the criterion for the Kármán vortex excitation is added for comparison. Solid curves in the figure show the contour line of the longitudinal vortex excitation region. Although the definition of Sc by equation (4.3) is based on the two dimensionality of the flows, Figure 17 gives a useful and clear comparison of the features of longitudinal vortex excitations with the Kármán vortex excitation as seen in the figure.

The difference in nature between the two longitudinal vortex excitations is also clearly seen in Figure 17. While the trailing vortex excitation is suppressed with a damping factor measured by $Sc = 28$, which is around one half of the maximum value for the Kármán vortex excitation [14], the necklace vortex excitation is observed at

$Sc = 150$, which corresponds to the maximum damping attained by the eddy current damper used in this experiment. The width of necklace vortex excitation range of $(f_{v0} - f_n)/f_n$ gradually decreases with Sc. When Sc is small it is much wider in the positive side than in the negative side. The lower limit of the range is almost constant at around -0.1 over the whole Sc range.

In contrast, the $(f_{v0} - f_n)/f_n$ region for the trailing vortex excitation expands wider in the negative side and the total width decreases rapidly in the range of $Sc = 20 - 25$.

(a) Trailing vortex excitation (*s/d*=0.08)
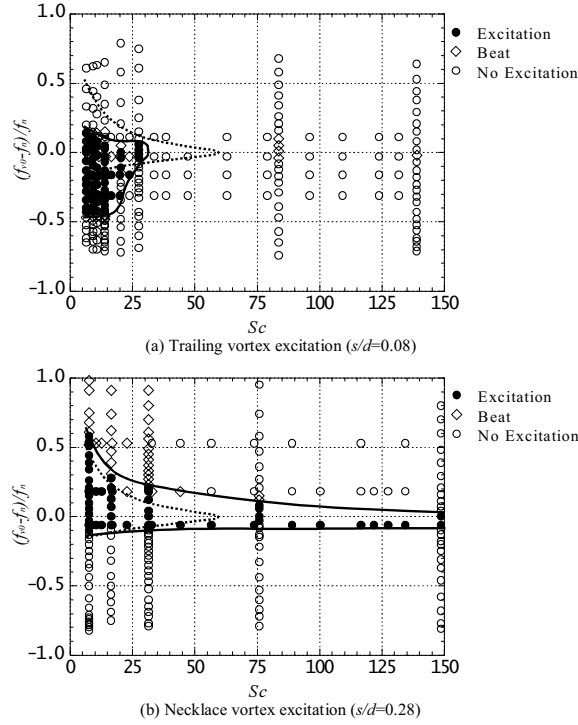
(b) Necklace vortex excitation (*s/d*=0.28)

Figure 17. Criterion for longitudinal vortex excitation. ($d = d_1 = d_2 = 26$ mm) Solid curve: Contour of longitudinal vortex excitation region. Broken curve: Contour of Kármán vortex excitation region.

Since the oscillation frequency of the upstream cylinder is fixed at its natural frequency over the whole longitudinal vortex excitation region, the oscillation is regarded as the resonance of a linear elastic system with small damping. Hence, the amplitude of excitation force is calculated by the following equation.

$$(C_{LR})_{rms} = \frac{8\pi St_n^2 m\delta}{\rho d^2 l} \cdot \sqrt{2}\left(\frac{Z_{rms}}{d}\right) \ . \tag{4.4}$$

Taking into account the fact that span-wise region where the fluctuating pressure caused by the longitudinal vortices is exerted is limited to R_T and R_N as shown in

Figure 9, the substantial alternating lift coefficients of the longitudinal vortices are proposed as defined by the following equations.

$$\text{Trailing vortex} \quad : \quad (C_{LR})'_{rms} = \frac{8\pi St_n^2 m\delta}{\rho d^2 \cdot 2R_T} \cdot \sqrt{2}\left(\frac{Z_{rms}}{d}\right) \qquad (4.5\text{a})$$

$$\text{Necklace vortex} \quad : \quad (C_{LR})'_{rms} = \frac{8\pi St_n^2 m\delta}{\rho d^2 \cdot 2R_N} \cdot \sqrt{2}\left(\frac{Z_{rms}}{d}\right) \qquad (4.5\text{b})$$

In addition to the measurements of oscillation amplitude with varying U at a fixed damping factor as shown in Figure 13, measurements were carried out with varying damping factor δ at a fixed velocity. The oscillation amplitude at the vortex excitation

(a) Trailing vortex excitation (s/d=0.08)

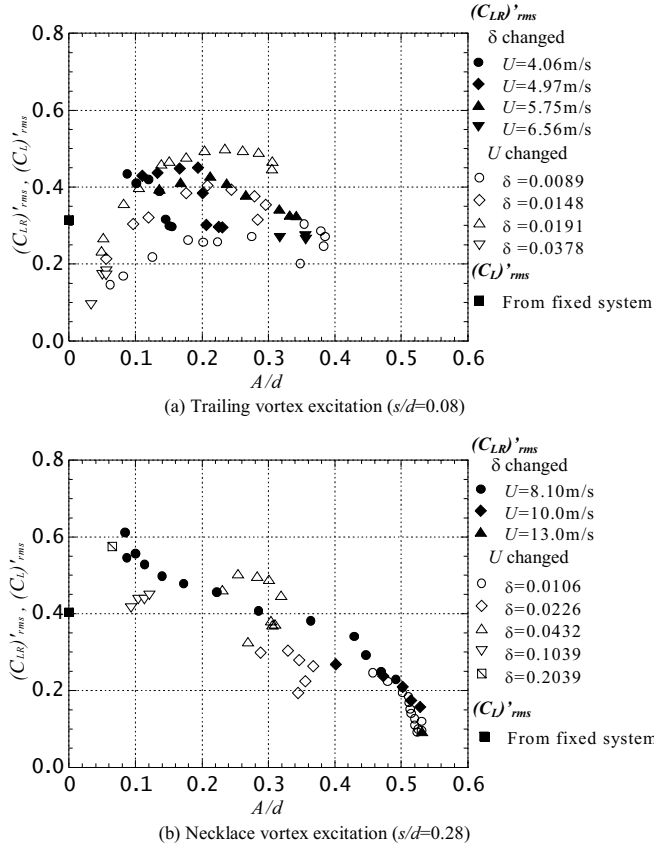(b) Necklace vortex excitation (s/d=0.28)

Figure 18. Substantial alternating lift coefficient due to longitudinal vortices ($d = d_1 = d_2 = 26$ mm)

is converted into the substantial alternating lift coefficient $(C_{LR})'_{rms}$ and plotted against the non-dimensional amplitude as shown in Figure 18, where results obtained for the fixed system presented in Figure 12 are also added. Note that the Reynolds

number varies for the fixed-δ measurements while it is constant for the fixed-U measurements.

$(C_{LR})'_{rms}$ for the necklace vortex seems to collapse on a single curve and decreases with the oscillation amplitude A/d. The maximum value appears at the smallest vortex excitation amplitude and has a value around 0.6, which is considerably larger than the value for the fixed system.

In contrast, $(C_{LR})'_{rms}$ for the trailing vortex scatters largely, and at the incidence of the vortex excitation $(C_{LR})'_{rms}$ is much smaller than that of the fixed system. It seems to increase with the oscillation amplitude till the maximum value 0.5 appears at around $A/d = 0.2$.

5. Conclusions

Comprehensive experiments are carried out to clarify the behavior of the longitudinal vortex excitations of the upstream cylinder in a cruciform two circular cylinder system in a uniform flow. Influences of the gap-to-diameter ratio, the diameter ratio of the two cylinders and the damping factor on the vortex shedding and the oscillation are investigated. Cross spectra of the velocities at properly selected two points near the crossing and measurements of the fluctuating lift force definitely reconfirmed and expanded the results so far reported by the present authors. The conclusions newly found in this work are summarized as follows.

1. The downstream cylinder diameter d_2 has a dominating influence on the longitudinal vortex structure formed near the crossing. That is, the trailing vortices shed when $0 < s/d_2 < 0.25$ and the necklace vortices shed when $0.25 < s/d_2 < 0.7$. The maximum value of s/d_2 for the necklace vortex shedding found in this work is considerably larger than reported so far.

2. Compared with the necklace vortex, the trailing vortex has a very irregular nature as follows. Its $St_0 - Re$ curve does not attain a constant value up to $Re = 40,000$, unlike the Kármán vortex or the necklace vortex, and has a large discontinuous jump at $Re = 5,000$. Under a fixed velocity f_{v0} changes irregularly with the gap s and there was found no coherent tendency in $f_{v0} - d_2$ relation.

3. The shedding area of the longitudinal vortex on the upstream cylinder surface is nearly proportional to the downstream cylinder diameter, and in turn, the alternating lift force caused by the longitudinal vortices is also proportional to the downstream cylinder diameter. Based on this result, the substantial lift coefficient of the longitudinal vortices is proposed to estimate the exciting force of the longitudinal vortices.

4. The criteria for the two longitudinal vortex excitations are presented as a curve on $Sc - (f_{v0} - fv)/f_n$ plane. The former parameter expresses the relative deviation of the natural vortex shedding frequency from the natural frequency of the upstream cylinder, and the latter is the Scruton number conventionally applied to two-dimensional flows. Compared with the Kármán vortex excitation of the same aspect ratio cylinder, the minimum value of Sc to suppress the trailing vortex excitation is smaller than that for the Kármán vortex. In contrast, the

necklace vortex excitation can occur even when Sc is three times as large as that to suppress the Kármán vortex excitation.

The criteria for the longitudinal vortex excitation in Figure 17 give the guideline for the occurrence of the excitation, and the substantial alternating lift coefficient given in Figure 18 can be applied to predict the vortex excitation amplitude for a system with an arbitrary aspect ratio. These results obtained in this work will be a guideline to predict and to avoid or suppress hazardous vibrations caused by longitudinal vortices.

REFERENCES

1. BISHOP, R.E.D. and HASSAN,A.Y.: *The lift and drag forces on a circular cylinder oscillating in a flowing fluid*, Proc. Royal Soc., London A-277, (1964), 51-57.

2. KOOPMAN, G.H.: *The vortex wakes of vibrating cylinders at low Reynolds numbers*, J. Fluid Mech., **28**, (1967), 501-518.

3. SARPKAYA, T.: *Vortex-induced oscillations*, Journal of Applied Mechanics, **46**, (1979), 241-258.

4. BEARMAN, P.W.: *Vortex shedding from oscillating bluff body*, Annual Review of Fluid Mechanics, **16**, (1984), 195-222.

5. TOMITA, Y., INAGAKI, S., SUZUKI, S. and MURAMATSU, H.: *Acoustic Characteristic of Two Circular Cylinders Forming a Cross in Uniform Flow (Effect on Noise Reduction and Flow Around Both Cylinders)*, JSME International Journal, 30-265, (1987), 1069-1079.

6. SHIRAKASHI, M., MIZUGUCHI, K. and BAE, H.M.: *Flow-induced excitation of an elastically-supported cylinder caused by another located downstream in cruciform arrangement*, J. of Fluids and Structures, **3**, (1989), 595-607.

7. SHIRAKASHI, M., BAE, H.M., SANO, M. and TAKAHASHI, T.: *Characteristics of periodic vortex shedding from two cylinders in cruciform arrangement*, J. of Fluids and Structures, **8**, (1994), 239-256.

8. SHIRAKASHI, M., SANO, M. and HIGASHI, K.: *Structure of vortices shedding periodically from two cylinders in cruciform arrangement*, ASME Separated and Complex Flows, **217**, (1995), 137-142.

9. TAKAHASHI, T., BARANYI, L. and SHIRAKASHI, M.: *Configuration and Frequency of Longitudinal Vortices Shedding from Two Circular Cylinders in Cruciform Arrangement*, Journal of the Visualization Society of Japan, 19-75, (1999), 328-336.

10. FOX, T.A.: *Flow Around Two Circular Cylinders Arranged Perpendicular to Each Other*, The Univ. of Queensland, Dep. of Civil Eng. Research Report, CE126, (1990).

11. HOSAKA, F.: *Proc. Visualization Society of Japan*, **16**(2), (1996), 159-162. (in Japanese)

12. SHIRAKASHI, M.: *An instructional fluids engineering experiment: Measurement of the Kármán vortex using HWA*, FED-Vol. 220, ASME, (1995), 13-17.

13. KUMAGAI, I.: *Influence of oscillation of upstream circular cylinder on flow around criss-cross circular cylinder*, Proc. JSME Annual meeting 1, 99-1, (1999-7), 471-472. (in Japanese)

14. SCRUTON, C.: *On the wind-excited oscillations of stacks, towers and masts*, Proc. Int. Conf. Wind Effects on Build. & Struc. (Teddington), Her Majesty's Stationary Office, Paper 16, (1963), 798-836.